Surface Science 615 (2013) 80–87

Contents lists available at SciVerse ScienceDirect

Surface Science

journal homepage: www.elsevier.com/locate/susc

Quantifying residual hydrogen adsorption in low-temperature STMs

F.D. Natterer, F. Patthey, H. Brune *

Institute of Condensed Matter Physics (ICMP), Ecole Polytechnique Fédérale de Lausanne (EPFL), Station 3, CH-1015 Lausanne, Switzerland

ARTICLE INFO

Article history:
Received 9 February 2013
Accepted 21 April 2013
Available online 25 April 2013

Keywords:
Hydrogen adsorption
Residual gas
Low-temperature scanning tunneling microscope
Kondo effect
Hexagonal boron nitride
Titanium

ABSTRACT

We report on low-temperature scanning tunneling microscopy observations demonstrating that individual Ti atoms on hexagonal boron nitride dissociate and adsorb hydrogen without measurable reaction barrier. The clean and hydrogenated states of the adatoms are clearly discerned by their apparent height and their differential conductance revealing the Kondo effect upon hydrogenation. Measurements at 50 K and 5×10^{-11} mbar indicate a sizable hydrogenation within only 1 h originating from the residual gas pressure, whereas measurements at 4.7 K can be carried out for days without H_2 contamination problems. However, heating up a low-*T* STM to operate it at variable temperature results in very sudden hydrogenation at around 17 K that correlates with a sharp peak in the total chamber pressure. From a quantitative analysis we derive the desorption energies of H_2 on the cryostat walls. We find evidence for hydrogen contamination also during Ti evaporation and propose a strategy on how to dose transition metal atoms in the cleanliest fashion. The present contribution raises awareness of hydrogenation under seemingly ideal ultra-high vacuum conditions, it quantifies the H_2 uptake by isolated transition metal atoms and its thermal desorption from the gold plated cryostat walls.

1. Introduction

The adsorption of hydrogen is the ongoing focus of intense studies in chemisorption/physisorption [1] in the context of heterogeneous catalysis and in the field of hydrogen storage.[1]

Concerning investigations with scanning tunneling microscopy (STM), modifications of the sample's electronic and magnetic properties through an interaction with hydrogen have been reported. Examples are the coverage dependent inelastic excitations detected in the differential conductance (dI/dV) of physisorbed hydrogen on a copper surface [2], the emergence of vibrational excitations in dI/dV for hydrogenated La, Cr, and Ce adatoms on Ag(100) [3], as well as the alteration of the magnetic characteristics (Kondo effect) of Co adatoms on Pt(111) upon hydrogen uptake [4]. Furthermore, molecular hydrogen was also studied for its role in providing ultra-high geometrical resolution in STM topographs [5,6].

The above investigations were carried out under ultra high vacuum (UHV), and some of the H-induced effects showed up unintentionally, before they were confirmed by deliberately dosing molecular hydrogen. This reflects the frequently encountered assumption of an ideal UHV environment in surface science studies with the consequence of being oblivious to a hydrogen presence. Molecular hydrogen, as a matter of fact, is the dominant constituent of the residual gas, even though large an effort is invested to efficiently remove it from the system, or to irrevocably trap the molecules, in order to attain the required low pressures in the 10^{-11} mbar range. The latter is ultimately limited by hydrogen desorption from the chamber walls and the release of hydrogen from filaments.

Little literature is devoted to quantify the unintended influence of hydrogen in a UHV system. In the present low temperature STM study, we investigate the hydrogen uptake by individual Ti adatoms on hexagonal boron nitride (*h*-BN) grown on Rh(111), where it exhibits a strong corrugated moiré pattern, and on Ni(111), where it forms a flat commensurate layer. In these model systems, significant differences between the STM appearance of hydrogenated and clean Ti adatoms allow to quantify the amount of hydrogen the sample is subject to under seemingly ideal UHV conditions. Hydrogenated Ti adatoms show a pronounced reduction of their apparent height, as well as a Kondo feature in dI/dV on the non-magnetic substrate that is absent on the clean species. We show that hydrogen encounters virtually no dissociation barrier upon impinging on the Ti adatom, which entails the formation of TiH, and presumably also to TiH_2, complexes. While measurements at 4.7 K can be carried out for days without signs of hydrogen contamination from the residual gas, investigations at 50 K suffer from a significant hydrogen uptake within only 1 h. The liquid helium cooled cryostat represents an efficient hydrogen pump at 4.7 K, preventing hydrogen from reaching the sample. When the low-temperature STM is operated at variable temperature by heating up the cryostat, hydrogen desorption sets in at 17 K, signifying a very low hydrogen adsorption energy and explaining why the cryostat ceases to act as a hydrogen pump at elevated temperatures. Furthermore, we show how H-contamination from the evaporator can be avoided and we demonstrate the removal of hydrogen from Ti adatoms through the electrical field of the STM tip.

* Corresponding author.
E-mail address: harald.brune@epfl.ch (H. Brune).

[1] www.hydrogen.energy.gov

0039-6028/$ – see front matter
http://dx.doi.org/10.1016/j.susc.2013.04.008

2. Experimental setup

The measurements were performed with a homemade low temperature STM, operating at 4.7 and 50 K and in a UHV chamber with a base pressure $p < 5 \times 10^{-11}$ mbar [7]. All pressure values refer to the readout of a N_2-calibrated ionization gauge. The Rh(111) [Ni(111)] single-crystal was cleaned by repeated cycles of Ar^+ ion sputtering (10 μA/cm^2, 1 kV, 300 K, 30 min), annealing in oxygen (815 K, 5 min, 2×10^{-7} mbar) and flash to 1450 K [1100 K]. The single layer *h*-BN was grown by chemical vapor deposition (CVD) in exposing the sample at 1040 K for 3 min to a borazine partial pressure of 2×10^{-6} mbar [8,9]. Due to the catalytic activity of the substrate, and to the inertness of the *h*-BN layer, the CVD growth is self-limiting to one monolayer [9].

Titanium atoms were deposited from a high purity rod with an e-beam evaporator while maintaining the pressure in the 10^{-11} mbar range and with the sample held in the STM position. The deposition flux was calibrated with STM by measuring the density of monomers obtained from statistical growth of very small coverages on the atomically clean Rh substrate. The necessary condition for statistical growth is that the adsorbed atoms are immobile at the deposition temperature of 10 K. Evidence for this is derived from the fact that we find only one ad-species after Ti deposition on Rh(111), and that this species does not move in consecutive STM images recorded at 4.7 K. At the low coverages used, this identifies them as monomers. The density of adsorbates is thus equivalent to the coverage. Coverages are given in monolayers (ML); one ML being defined as one adatom per Rh or Ni substrate atom, respectively.

Molecular hydrogen was dosed by backfilling the UHV chamber to a given partial pressure with a leak valve and leaving the cryostat's thermal shield open to permit direct exposure of the sample in the STM position. The exposure is given in Langmuirs, 1 L = 1.33×10^{-6} mbar s. The STM images were acquired at constant current, and the indicated tunnel voltages (V_t) correspond to the sample potential. Scanning tunneling spectroscopy (STS) was performed by recording the bias-dependent differential conductance using a lock-in amplifier and adding a sinusoidal 2 mV peak-to-peak modulation at 397 Hz to the bias voltage.

3. Results and discussion

3.1. Hydrogen from the evaporator

Fig. 1 shows STM images of the surfaces after deposition of per mill amounts of Ti at 10 K onto (a)–(b) *h*-BN/Rh(111)–(12 × 12) [8,10–13] and (c) *h*-BN/Ni(111)–(1 × 1) [9]. On all samples, individual protrusions are randomly distributed about the surface. They appear with two distinct heights of around 150 and 330 pm, as it becomes evident from the lower histogram on the left hand side in (d) and from the two line cuts in (e). The fraction of low apparent height adsorbates is significantly reduced from (a) to (b) due to an improvement of the evaporation conditions. For both experiments we have used a thoroughly degassed Ti source, however, in (a) the pressure during evaporation has been in the low 10^{-10} mbar range, while for Fig. 1(b) and (c) we had performed several preliminary depositions onto the closed radiation shield of the cryostat with open evaporator shutter at 1.5–2 times higher flux such as to stay in the 10^{-11} mbar range during the evaporation onto the sample. This way the surface of the Ti rod is degassed at slightly higher temperature than the one used for the subsequent evaporation and the pumping of the evaporator is more efficient with the shutter open. The same holds for Ti deposition on *h*-BN/Ni(111), shown in Fig. 1(c) for the improved deposition routine. As will become evident below, the adsorbates appearing with small height in constant current STM images are hydrogenated Ti atoms and the ones appearing as 330 pm tall protrusions are clean ones. Therefore commonly used deposition conditions lead to a hydrogenation of roughly half of the adsorbates, while surfaces with 98% clean Ti atoms can be created by putting special care on the evaporation conditions.

We note that on *h*-BN/Rh(111)–(12 × 12) the Ti atoms are located between the moiré depressions and the connected protruding areas, also referred to as wires [8]. We observe that the adsorbates are immobile at the imaging temperature of 4.7 K on both samples; for *h*-BN/Rh this is in accordance with former observations of individual molecules [8,12,14,15], rare gas [16,17], and transition metal adatoms [18].

The assignment of each protrusion to a single Ti atom comes from the evaluation of the mean cluster size as being close to one atom. We follow the procedure outlined in ref. [18] that also yields the initial sticking coefficient s_0. The sample of Fig. 1(a) has been on purpose only partly covered by *h*-BN. On the clean Rh(111) parts we determined the Ti coverage to be $\Theta = (8.1 \pm 0.4) \times 10^{-4}$ ML. If this coverage were also present on the *h*-BN areas, one would expect a fraction of empty moiré unit cells, with size $n = 144$ Rh(111) unit cells, of $P_0 = (1-\Theta)^n = (0.890 \pm 0.005)$. However, we observe with (0.906 ± 0.005) a slightly, but significantly larger fraction of empty cells. This fraction is obtained for a coverage of $\Theta = (6.9 \pm 0.3) \times 10^{-4}$ ML. Therefore the coverage on *h*-BN/Rh(111) is significantly lower and the initial sticking coefficient is $s_0 = (0.85 \pm 0.09)$ for Ti deposited onto this surface at 10 K. From the ratio of coverage and density we determine a mean cluster size per protrusion of (1.05 ± 0.10) atoms in Fig. 1(a) and thus the protrusions are almost exclusively individual Ti adatoms, either hydrogenated or not. For the case of *h*-BN/Ni(111), we compared adsorbate densities on clean Ni and *h*-BN covered surface areas and derived $s_0 = (0.8 \pm 0.1)$. In accordance with these results, initial sticking coefficients below one have been reported for transition metal adatoms on *h*-BN/Ni(111)–(1 × 1) [19] and on *h*-BN/Rh(111)–(12 × 12) [18].

3.2. Hydrogen dosage

From the above observations we conclude that each of the adsorbate induced protrusions in Fig. 1(a), (b), and (c) contains a single Ti adatom. The evidence that one of the two species is a clean and the other a hydrogenated Ti adatom is derived from exposing a sample with mostly Ti atoms in the high apparent height state to a partial pressure of molecular hydrogen. Fig. 2 shows that dosing 1 L H_2 at 10 K leads to a drop of the adsorbates apparent height from (330 ± 16) in (a) to (110 ± 20) pm in (b), clearly identifying the latter as the hydrogenated species. In addition to the Ti adsorbates, the STM images show *h*-BN point defects (one has been labeled d) that exhibit a marked contrast inversion upon hydrogen adsorption, presumably due to a H atom in the tunnel junction [5,6]. The line defect in Fig. 2(a) is a *h*-BN domain wall where the stacking of the B atoms with respect to the substrate changes from fcc to hcp; note that the N atom are always at on-top sites [20,21].

3.3. STM-induced hydrogen desorption from Ti adatoms

It is possible to remove hydrogen from the Ti host atom via tip manipulation. A *h*-BN/Rh(111)–(12 × 12) sample with a majority of hydrogenated Ti adatoms is shown in Fig. 3(a). A bias pulse of +4 V applied for 50 ms at open feedback loop with the tip centered above the position marked by × removes virtually all hydrogen from Ti adatoms located within a radius of about 40 nm, see Fig. 3(b). The larger the pulse amplitude the larger the desorption region, i.e., there is a monotonous correlation of the H-removal radius and the voltage pulse. Radii of the order of 100 nm have been observed with voltage pulses up to +8 V. The latter, however, frequently involved undesired tip-changes. We note that the voltage pulse mediated hydrogen desorption equally works for the hydrogenated Ti adatoms on *h*-BN/Ni(111).

3.4. Hydrogen induced Kondo effect

In addition to the different apparent height, hydrogenated and clean Ti atoms adsorbed onto *h*-BN/Rh clearly distinguish themselves

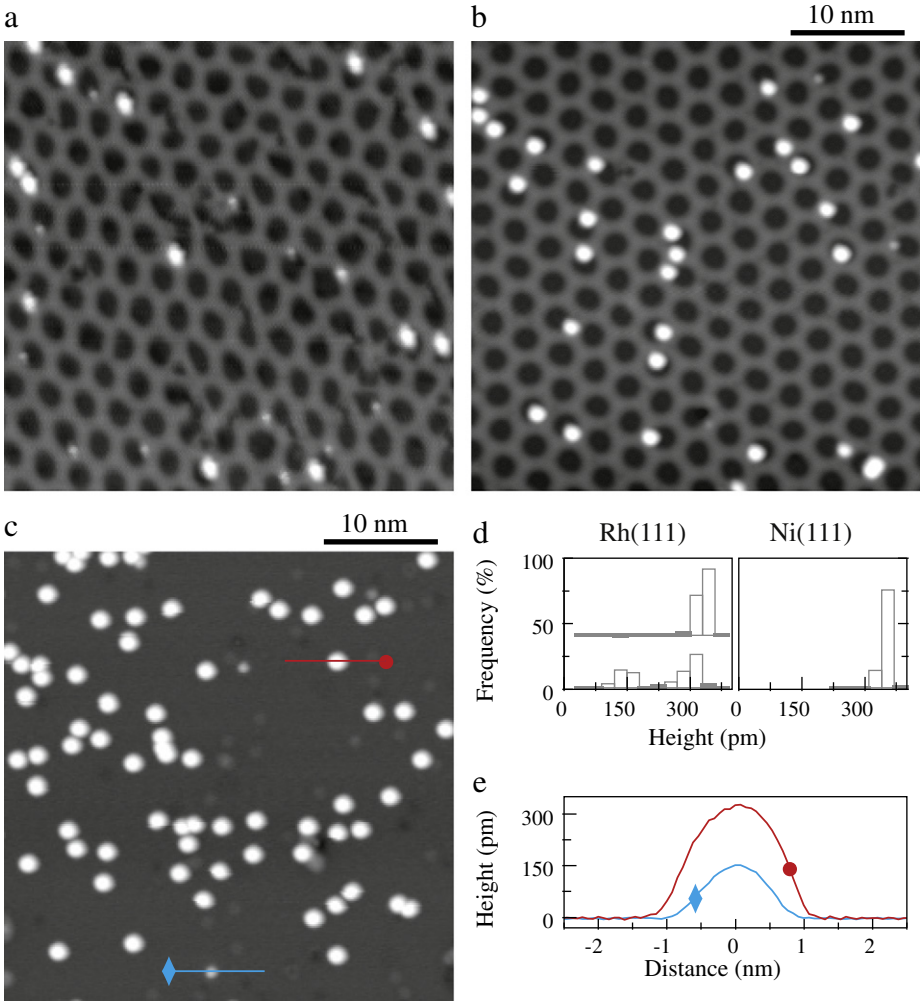

Fig. 1. (a) Coexistence of clean and hydrogenated Ti atoms on *h*-BN/Rh(111)–(12 × 12) discerned by their apparent heights [$\Theta = (6.9 \pm 0.3) \times 10^{-4}$ ML, $V_t = -100$ mV, $I_t = 20$ pA]. (b) Improving the degassing routine of the evaporator increases the fraction of clean Ti atoms to more than 90% [$\Theta = (1.2 \pm 0.1) \times 10^{-3}$ ML, $V_t = -50$ mV, $I_t = 20$ pA]. (c) Clean and hydrogenated Ti adatoms are also found for Ti deposition on *h*-BN/Ni(111) [$\Theta = (2.3 \pm 0.1) \times 10^{-3}$ ML, $V_t = -100$ mV, $I_t = 10$ pA]. (a), (b), and (c) $T_{dep} = 10$ K and $T_{STM} = 4.7$ K. (d) Apparent height histograms of the Ti adsorbates for the samples shown in (a) bottom left, (b) top left, and (c) right. (e) Line profile across a clean (•) and hydrogenated (♦) Ti adatom.

in their *dI*/*dV* spectra. Fig. 4 shows that the differential conductance of clean Ti adatoms is basically featureless, whereas the hydrogenated one exhibits a distinct zero-bias resonance with a 100% conductance increase. A voltage pulse of + 1.2 V on the adatom showing the resonance removes hydrogen and concomitantly resets the *dI*/*dV* to the featureless one characterizing the clean Ti adatom, see Fig. 4(c) and (d).

The peak at the Fermi level (E_F) is attributed to a Kondo feature [22,23]. Below the Kondo temperature T_K, the magnetic moment of a localized magnetic impurity is screened collectively by the surrounding conduction electrons of the non-magnetic host. The spectral line shape of the Kondo feature arises from the interference of electrons tunneling directly into the impurity state with the ones tunneling into the continuum. It is described by a Fano function [23–25]:

$$\frac{dI}{dV}(V) \propto \frac{(q+\epsilon)^2}{1+\epsilon^2}, \epsilon = \frac{eV-\epsilon_0}{\Gamma}. \quad (1)$$

Γ describes the half-width at half-maximum (HWHM) of the resonance, q the ratio of tunneling into the impurity versus the continuum, and ϵ_0 gives the position of the impurity state with respect to E_F [23–26].

The recorded *dI*/*dV* curve was fitted by iteratively adjusting the Fano line-shape parameters and subsequent convolution with the function of thermal and modulation broadening [27,28]. The sample and tip temperatures were hereby assumed to be equal to 4.7 K. The result of this procedure is shown as full black line in Fig. 4(c). It is in excellent agreement with experiment and yields $\Gamma = (2.8 \pm 0.2)$ meV and $q = (4.15 \pm 0.05)$.[2]

From these parameters we ultimately extract the intrinsic Kondo temperature of $T_K = (29 \pm 3)$ K through $\Gamma = \sqrt{(\pi k_B T)^2 + (k_B T_K)^2}$ [25,29], where T is the sample temperature of 4.7 K, and k_B the Boltzmann constant.[3] A Kondo resonance in STS was reported for Ti atoms adsorbed on Au(111) [30], on Ag(100) [25], and on Cu_2N/Cu(100) [29]. In the present case, this resonance becomes apparent only after hydrogenation of the Ti adatom. Hydrogen may change the charge state and thereby the spin of the adatom, but also its magnetic anisotropy. Both may be involved in the appearance of the Kondo effect [4]. We note that the H-induced Kondo effect reported here for Ti atoms on *h*-BN is not observed on Ni(111), presumably due to the high spin-polarization at E_F [21] that is preventing the spin-flip scattering of the conduction electrons.

3.5. Hydrogen uptake by titanium adatoms

The hydrogen uptake by an ensemble of Ti atoms adsorbed onto *h*-BN/Ni(111) has been monitored at 50 K by recording consecutive

[2] The errors were determined by manually varying the fit parameters until the disagreement with the measured conductance became significant.

[3] The formula is expressed for HWHM and the factor α from Ref. [29] is set equal to 2π, in agreement with Ref. [25].

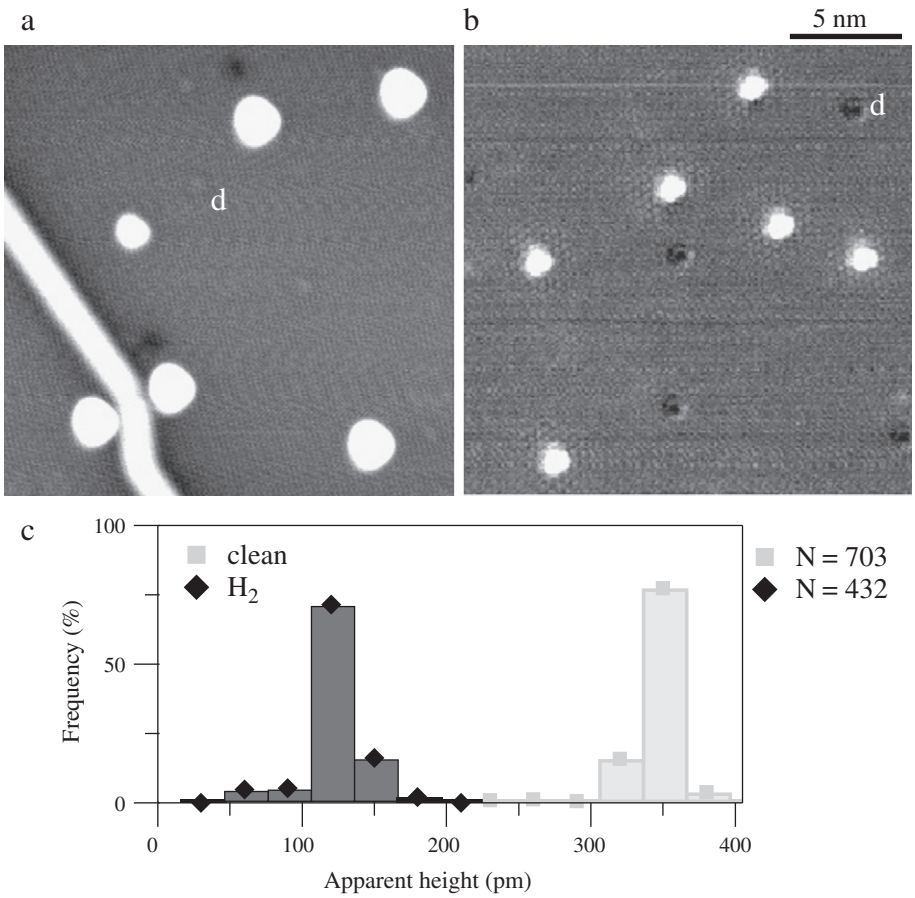

Fig. 2. Sample with Ti adatoms on *h*-BN/Ni(111) before (a) and after (b) 1 L hydrogen exposure at 10 K ($V_t = -100$ mV, $T_{STM} = 4.7$ K, (a) $I_t = 210$ pA, (b) $I_t = 20$ pA). (c) Superimposed apparent height histogram of Ti adatoms before and after exposure to molecular hydrogen with the respective numbers of analyzed events indicated on the right.

STM images of the same surface region over 6 h. The result is shown in Fig. 5. The first image depicts the surface shortly after deposition. Almost all the Ti adatoms are in their clean state and imaged as 300 pm high protrusions, in agreement with the experiment at 4.7 K. With elapsing time, a clear surface evolution can be observed. After only 1 h almost 50% of the Ti adatoms are hydrogenated and appear with the reduced height. Five more hours later one encounters only traces of clean Ti adatoms. The relative abundance of clean Ti atoms over time is shown in Fig. 5(d). It is perfectly fitted by the expected exponential decay $n/n_0 = exp(-t/\tau)$ and yields a decay constant of $\tau = (7.7 \pm 0.5) \times 10^3$ s. We recall the low residual pressure of $p = 5 \times 10^{-11}$ mbar. Working under these conditions is generally assumed to be sufficiently good for observation times of a few hours for a sample in its clean state, and a co-adsorption of residual gas is often disregarded.

In order to derive an estimate of the sticking coefficient for molecular hydrogen on individual transition metal adatoms, in our case on

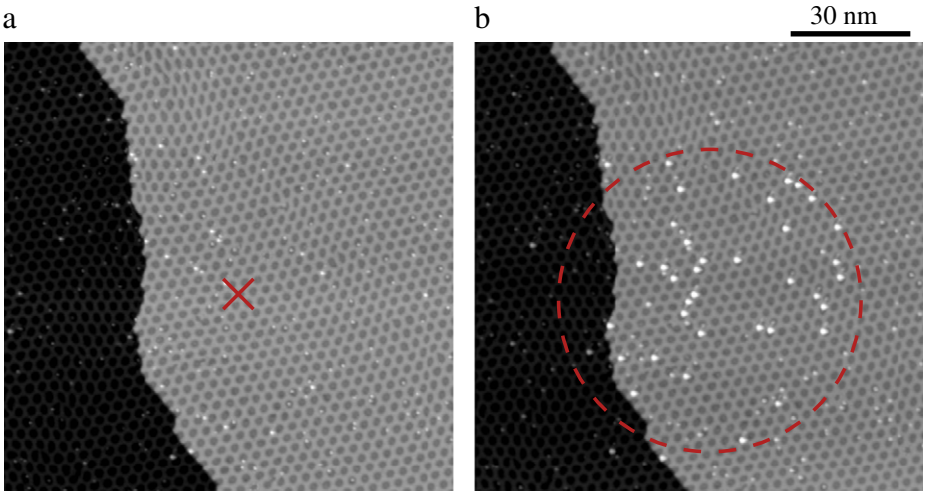

Fig. 3. Hydrogen removal from an ensemble of hydrogenated Ti adatoms by a bias pulse of +4 V and 50 ms duration applied at the indicated position (×) with open feedback loop. STM image (a) before and (b) after bias pulse ($V_t = -100$ mV, $I_t = 20$ pA, $\Theta = (1.2 \pm 0.2) \times 10^{-3}$ ML).

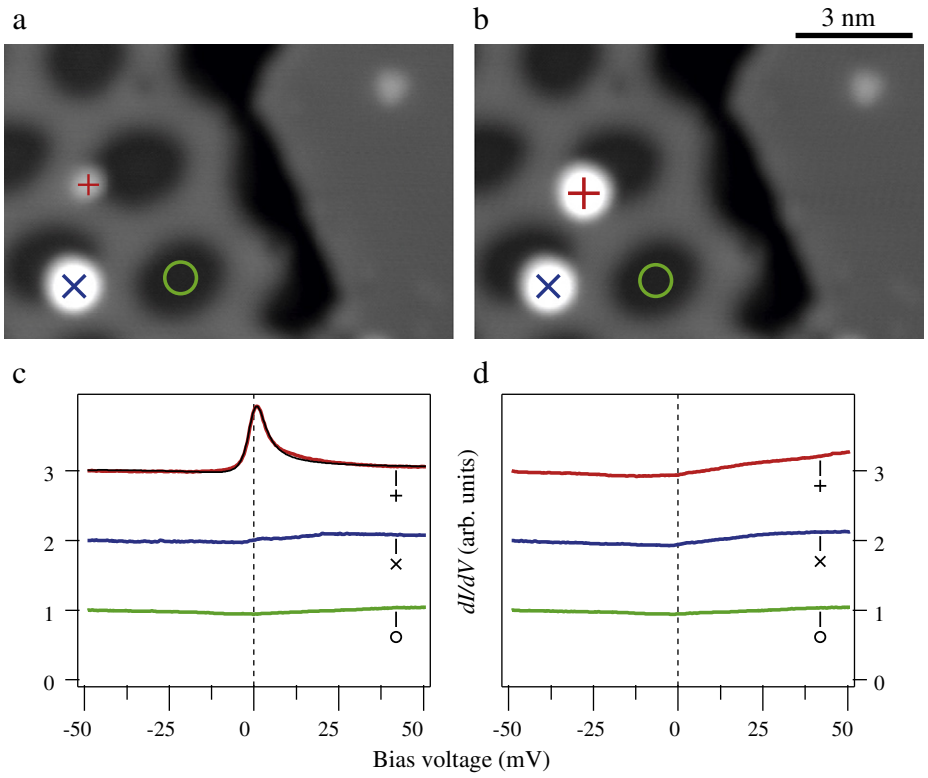

Fig. 4. STM images of two Ti adatoms on *h*-BN/Rh(111). (a) One atom is clean (×) and one hydrogenated (+). (b) Both atoms are clean after removing the H with a +1.2 V pulse above (+) ($V_t = -100$ mV, $I_t = 20$ pA). (c) The hydrogenated Ti adatom exhibits a Kondo resonance in *dI*/*dV* that is (d) absent for the clean Ti adatom (set point before opening the feedback-loop: $V_t = -50$ mV and $I_t = 200$ pA). The full black line in (c) shows a fit with a Fano function. The spectra are normalized to the conductance at −50 mV and vertically offset by one unit. The right hand side in (a)–(b) shows the coexisting Rh(111) surface termination.

Ti/*h*-BN/Ni(111)–(1 × 1), we consider the impingement rate per unit area of a gas of molecules with mass *m*, at pressure *p*, and temperature *T*:

$$R = \frac{p}{\sqrt{2\pi m k_B T}}. \quad (2)$$

For our conditions of $p = 5 \times 10^{-11}$ mbar, $T = 50$ K, and taking into account the fact that the residual gas is dominated by H_2, this yields $\nu = 7.1 \times 10^{-5}\ s^{-1}$ per Ni(111) site ($A_{Ni(111)} = 5.377 \times 10^{-20}\ m^2$) with $\nu = RA$. This rate translates to a mean time between subsequent impingements of $\tau' = 1.4 \times 10^4$ s. One immediately sees that τ' and τ differ only by a factor of 2; considering the ionization gauge sensitivity of 0.5 [31,32] for H_2 brings them to coincidence.

In this analysis, however, two more issues should be alluded to. The first is the thermal transpiration factor between the poorly connected volumes of the surrounding UHV chamber and the inner volume of the cryostat that entails a pressure ratio of $\sqrt{T_{in}/T_{out}}$, where T_{in} and T_{out} denote the gas temperature inside the cryostat and at the ionization gauge, respectively. Another aspect is the destiny of the second H atom after the dissociation of the molecule over the Ti adatom. The first sticks to the Ti atom, while the second may either desorb or migrate over the *h*-BN surface to the next clean Ti adatom and hydrogenate it. In the latter case, with $T_{in}/T_{out} = 6$, and the ionization gauge sensitivity of 0.5, we derive from the measured decay time a pressure readout of $(5.6 \pm 0.4) \times 10^{-11}$ mbar, in agreement with the indicated base pressure.

Therefore H_2 molecules arriving at the Ti adatoms are dissociated virtually with unit efficiency. This can be rationalized as follows. In general, the *d* holes characterizing bulk transition metals mediate hydrogen dissociation [33]. Furthermore, the dissociation ability of a transition metal surface is considerably enhanced at low-coordinated atoms such as steps [1,34]. For isolated transition metal atoms, such as Ni, hydrogen dissociation takes place via a charge transfer from the TM host to the anti-bonding states of the molecule, which will increase the H–H separation and ultimately lead to its dissociation [35,36]. While our data are suggestive for one H atom per Ti host, a close inspection of the apparent height distribution using a smaller bin size than in Fig. 2(c) reveals two peaks for the hydrogenated species, one centered at 110 and the other at 150 pm, which may be a signature of coexisting TiH and TiH_2 complexes. Hydrogen molecules hitting the *h*-BN layer at 50 K are scattered back into the vacuum without interfering with clean Ti atoms. We observe physisorption of molecular hydrogen only at 10 K. It manifests itself by patches of a $\left(\sqrt{3} \times \sqrt{3}\right)R30^{\circ}$ superstructure fixed around the Ti adatoms in Fig. 2(b) [37].

3.6. Hydrogen desorption from cryostat walls

After having quantified the H-uptake by Ti atoms adsorbed onto *h*-BN films, we can use such samples as very sensitive H detector inside the STM. Low-*T* STMs are sometimes used at variable temperature by letting the cryostat heat itself up after boiling off the cryogen. It is of interest at which sample temperature and how fast the sample gets H-contaminated under these circumstances. We address this question for our microscope. Once the cryogen is completely boiled off, the temperature rises with 2.3 m K s^{-1}, which is sufficiently slow to enable drift-compensation and therefore to stay on the same microscopic surface spot in a temperature range of 4.7–43 K. These values refer to the cryostat temperature. The sample is slightly cooler than this while heating. The temperature evolution of the number of clean versus hydrogenated Ti atoms is shown in Fig. 6.

In the initial state at 4.7 K, 98% of the atoms are clean and only 2% hydrogenated, see Fig. 6(a). For temperatures up to 16.0 K, the sample cleanliness remains unchanged, until at 16.3 K the apparent heights of the Ti adatoms suddenly drop to the value characteristic of hydrogenated Ti atoms, see Fig. 6(b). Fig. 6(c) shows that this

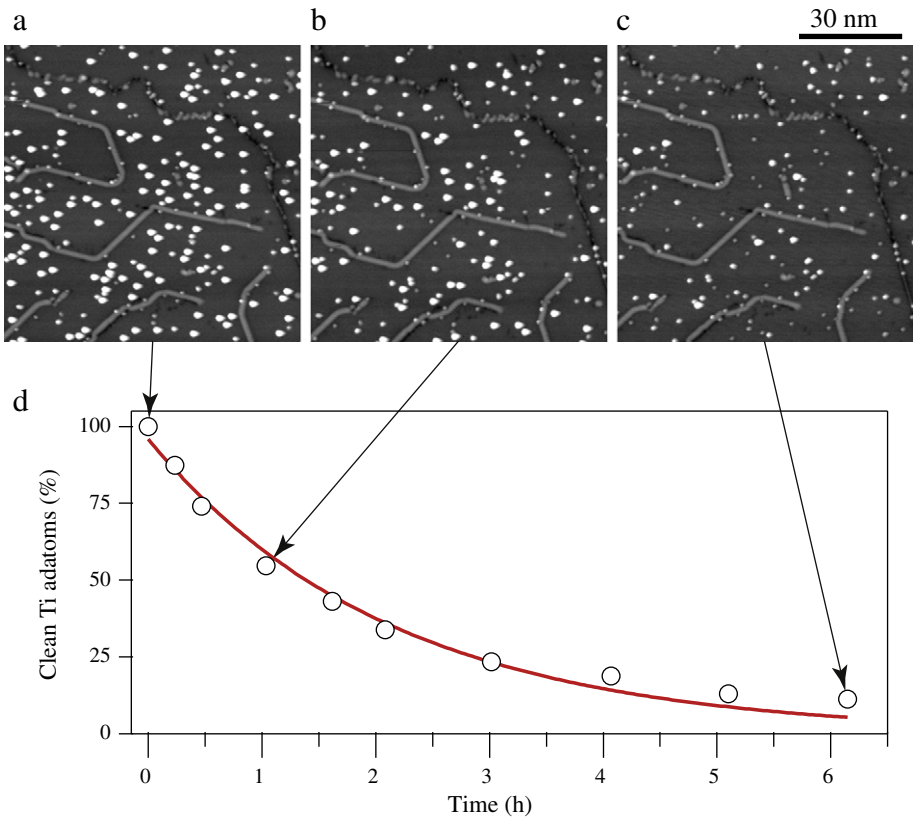

Fig. 5. Hydrogen uptake by Ti adatoms on *h*-BN/Ni(111) at 50 K. (a) In the initial state, most of the Ti adatoms are clean and appear as bright protrusions. Progressive increase of the abundance of adsorbates appearing with lower height after (b) 1 h and (c) 6 h exposure to the residual gas. (d) Exponential decrease of fraction of clean Ti adatoms versus time [$p = 5 \times 10^{-11}$ mbar, $V_t = -100$ mV, $I_t = 10$ pA, $\Theta = (2.8 \pm 0.5) \times 10^{-3}$ ML].

transition occurs over only 0.5 K or 220 s. The chamber pressure shown in Fig. 6(d) exhibits a sharp peak centered at 17 K and therefore at comparable, but slightly higher temperature. This peak arises from H_2-desorption off the cryostat walls. Its height reflects the experimental history preceding the warming up of the cryostat. By way of example, the pressure traces in Fig. 6(d) represent, from bottom to top, one day holding time, three days holding time, and the deliberate exposure to 1 L hydrogen before boiling off the cryogen.

The pressure evolution is reminiscent of thermal desorption spectroscopy (TDS) [38,39]. The desorption takes place from the gold plated copper walls of the cryostat. Since this is a polycrystalline surface, a distribution of adsorption sites with different desorption energies is expected. We therefore apply the method of Barrie [40] and fit the highest pressure peak to a normal distribution of desorption temperatures $(\mu \pm \sigma) = (18 \pm 4)$ K. The fit is shown as light-red curve in Fig. 6(d). It agrees very well with experiment and yields a desorption energy distribution of (52 ± 11) meV, under the assumptions of a common attempt frequency of 10^{13} Hz and a coverage independent desorption energy. In the view of the available TDS resolution and the slow heating rate β, that may allow for hydrogen re-adsorption, this low mean desorption energy has to be treated cautiously. Nonetheless, it reflects the very weak binding of hydrogen to the Au plating that is suggestive of a physisorbed molecular state.

We now compare the H_2 exposure of the sample resulting from the pressure peak with the one needed to explain the fast observed uptake. The exposure is obtained by integrating the surface impingement rate ν per Ni site in the considered temperature interval $[T_0,T_E]$:

$$D = \int_{t_0}^{t_E} \nu(t)\, dt = \beta \int_{T_0}^{T_E} \nu(T)\, dT, \tag{3}$$

where D is expressed in Langmuirs. The fraction of hit surface sites in the course of dosing D Langmuir of H_2 is given by $\nu = 1 - exp(-D)$. The integration of curve □, for instance, yields a dose of 2.6 L and concomitantly 93% of all surface sites have been hit during the overall temperature rise from 5 to 35 K. For the fast switching of Ti adatoms at 16.3 K, an equal or larger amount has to hit the sample within only 0.5 K. We recall that the above analysis has been performed for the volume outside the cryostat and the actual exposure the sample is subject to is expected to be significantly higher owing to the bad connection of the inner cryostat to the surrounding UHV vessel. A simple estimate shows that the pressure difference can amount to several orders of magnitude when considering the physical dimensions of the cryostat. By way of example, pre-covering the internal cryostat walls (500 cm^2) by 1/100 ML hydrogen gives rise to a partial pressure inside the 1 l volume of the cryostat of 2.6×10^{-5} mbar for a gas temperature of 20 K and without leakage. The fast switching thus already occurs at the leading edge of desorption and explains why the transition temperature slightly shifts from one experiment to another and why it is generally higher than the temperature where the hydrogenation of the Ti adatoms is observed.

4. Conclusions and outlook

The interaction with hydrogen has dramatic effects not only on the topography of Ti adatoms but also on their electronic properties on metal supported *h*-BN. It was shown that a base pressure in the 10^{-11} mbar range is not sufficient in preventing a hydrogen co-adsorption if the innermost radiation shields of the low-*T* STM are at 50 K. Consequently, experiments that are sensitive to hydrogen cannot be reasonably carried out at 50 K. However, no measurable H-contamination is detected when monitoring Ti adatoms at 4.7 K, i.e., the pressure inside the liquid helium cooled radiation shield is well below 10^{-14} mbar [41]. Our quantitative analysis yields that every H_2 molecule hitting a Ti atom gets dissociated without

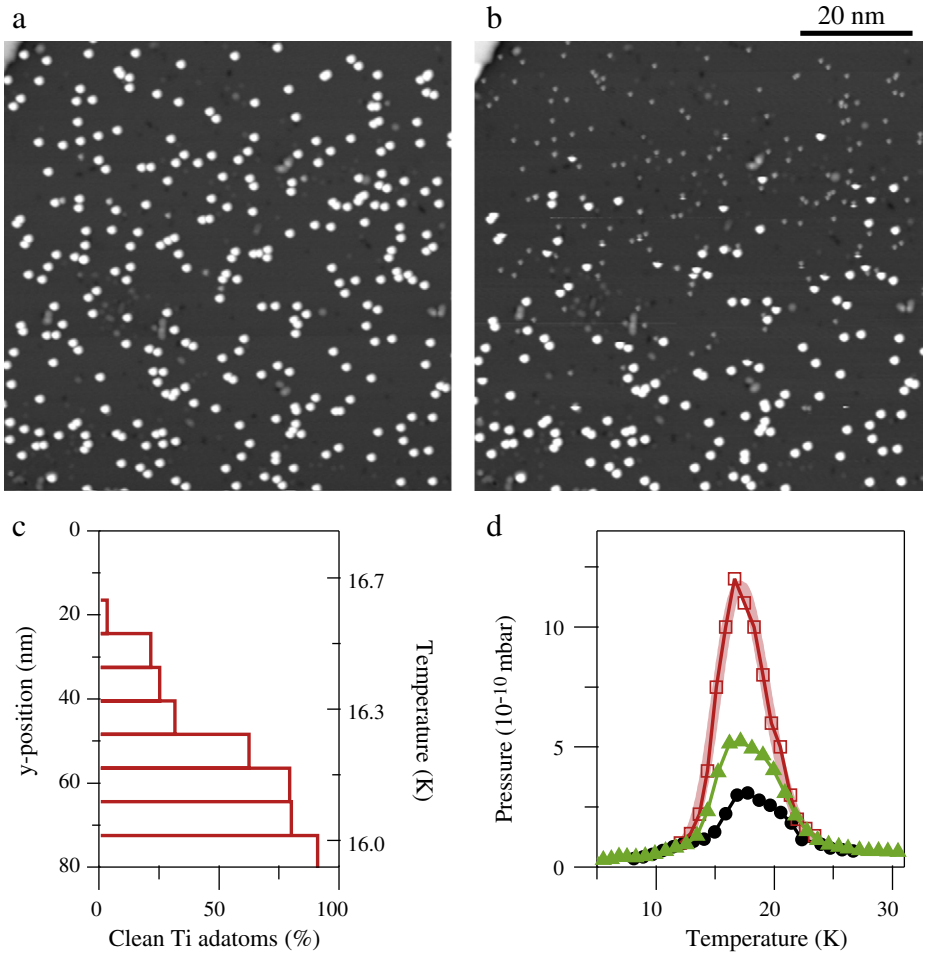

Fig. 6. H_2 desorption from cryostat walls while increasing the sample temperature. (a) Initial state with 98% clean Ti adatoms on *h*-BN/Ni(111) at 4.7 K. (b) Same surface region showing sudden hydrogenation at 16.3 K, scan from bottom to top. (c) Fraction of clean Ti adatoms as function of scan position in (b), respectively, STM temperature. (d) Residual gas pressure during increase of STM temperature for three experiments with different histories; see text. [$V_t = -100$ mV, $I_t = 20$ pA, and $\Theta = (2.3 \pm 0.3) \times 10^{-3}$ ML].

activation energy and at least one of its constituents gets adsorbed. Hydrogen molecules hitting the *h*-BN substrate at 50 K get reflected back into the gas phase, while at 4.7 K they form a physisorbed $\left(\sqrt{3} \times \sqrt{3}\right)$ phase condensing around point defects such as the Ti adatoms. The similarity between *h*-BN and graphene renders the discussed hydrogen interaction of adsorbed TM atoms relevant also to the growing field of epitaxial graphene and of its doping with adsorbates. In particular, when investigating magnetic properties with spatially integrating techniques, such as X-ray magnetic circular dichroism, one possibly studies hydrogenated species coexisting with the clean ones. However, also local probe measurements on individual adatoms have to be carried out with vigilance against hydrogen adsorption. For the present system Ti/*h*-BN it takes place without measurable dissociation barrier.

Acknowledgments

We gratefully acknowledge funding from the Swiss National Science Foundation.

References

[1] K. Christmann, Surf. Sci. Rep. 9 (1988) 1.
[2] J.A. Gupta, C.P. Lutz, A.J. Heinrich, D.M. Eigler, Phys. Rev. B 71 (2005) 115416.
[3] M. Pivetta, M. Ternes, F. Patthey, W.-D. Schneider, Phys. Rev. Lett. 99 (2007) 126104.
[4] Q. Dubout, F. Calleja, M. Etzkorn, F. Donati, A. Lehnert, L. Claude, P. Gambardella, H. Brune, Hydrogen-induced Kondo Effect for Single Cobalt Atoms on Pt(111), 2013. (in preparation).
[5] R. Temirov, S. Soubatch, O. Neucheva, A.C. Lassise, F.S. Tautz, New J. Phys. 10 (2008) 053012.
[6] C. Weiss, C. Wagner, C. Kleimann, M. Rohlfing, F.S. Tautz, R. Temirov, Phys. Rev. Lett. 105 (2010) 086103.
[7] R. Gaisch, J.K. Gimzewski, B. Reihl, R.R. Schlittler, M. Tschudy, W.-D. Schneider, Ultramicroscopy 42–44 (1992) 1621.
[8] M. Corso, W. Auwärter, M. Muntwiler, A. Tamai, T. Greber, J. Osterwalder, Science 303 (2004) 217.
[9] A. Nagashima, N. Tejima, Y. Gamou, T. Kawai, C. Oshima, Phys. Rev. B 51 (1995) 4606.
[10] O. Bunk, M. Corso, D. Martoccia, R. Herger, P.R. Willmott, B.D. Patterson, J. Osterwalder, J.F.v.d. Veen, T. Greber, Surf. Sci. 601 (2007) L7.
[11] R. Laskowski, P. Blaha, T. Gallauner, K.H. Schwarz, Phys. Rev. Lett. 98 (2007) 106802.
[12] S. Berner, M. Corso, R. Widmer, O. Gröning, R. Laskowski, P. Blaha, K. Schwarz, A. Goriachko, H. Over, S. Gsell, M. Schreck, H. Sachdev, T. Greber, J. Osterwalder, Angew. Chem. Int. Ed. 46 (2007) 5115.
[13] A.B. Preobrajenski, A.S. Vinogradov, M.L. Ng, E. Ćavar, R. Westerström, A. Mikkelsen, E. Lundgren, N. Mårtensson, Phys. Rev. B 75 (2007) 245412.
[14] H. Ma, T. Brugger, S. Berner, Y. Ding, M. Iannuzzi, J. Hutter, J. Osterwalder, T. Greber, ChemPhysChem 11 (2010) 399.
[15] Y. Ding, M. Iannuzzi, J. Hutter, J. Phys. Chem. C 115 (2011) 13685.
[16] H. Dil, J. Lobo-Checa, R. Laskowski, P. Blaha, S. Berner, J. Osterwalder, T. Greber, Science 319 (2008) 1824.
[17] R. Widmer, D. Passerone, T. Mattle, H. Sachdev, O. Gröning, Nanoscale 2 (2010) 502.
[18] F.D. Natterer, F. Patthey, H. Brune, Phys. Rev. Lett. 109 (2012) 066101.
[19] W. Auwärter, M. Muntwiler, T. Greber, J. Osterwalder, Surf. Sci. 511 (2002) 379.
[20] W. Auwärter, M. Muntwiler, J. Osterwalder, T. Greber, Surf. Sci. 545 (2003) L735.
[21] G.B. Grad, P. Blaha, K. Schwarz, W. Auwärter, T. Greber, Phys. Rev. B 68 (2003) 085404.
[22] A.C. Hewson, The Kondo Problem to Heavy Fermions, Cambridge University Press, 1993.

[23] V. Madhavan, W. Chen, T. Jamneala, M.F. Crommie, N.S. Wingreen, Science 280 (1998) 567.
[24] U. Fano, Phys. Rev. 124 (1961) 1866.
[25] K. Nagaoka, T. Jamneala, M. Grobis, M.F. Crommie, Phys. Rev. Lett. 88 (2002) 077205.
[26] V. Madhavan, W. Chen, T. Jamneala, M.F. Crommie, N.S. Wingreen, Phys. Rev. B 64 (2001) 165412.
[27] J. Klein, A. Léger, M. Belin, D. Défourneau, M.J.L. Sangster, Phys. Rev. B 7 (1973) 2336.
[28] M. Pivetta, F. Silly, F. Patthey, J.P. Pelz, W.-D. Schneider, Phys. Rev. B 67 (2003) 193402.
[29] A.F. Otte, M. Ternes, K.v. Bergmann, S. Loth, H. Brune, C.P. Lutz, C.F. Hirjibehedin, A.J. Heinrich, Nat. Phys. 4 (2008) 847.
[30] T. Jamneala, V. Madhavan, W. Chen, M.F. Crommie, Phys. Rev. B 61 (2000) 9990.
[31] S. Dushman, A.H. Young, Phys. Rev. 68 (1945) 278.
[32] D. Alpert, J. Appl. Phys. 24 (1953) 860.
[33] J. Harris, S. Andersson, Phys. Rev. Lett. 55 (1985) 1583.
[34] S. Dahl, A. Logadottir, R.C. Egeberg, J.H. Larsen, I. Chorkendorff, E. Törnqvist, J.K. Nørskov, Phys. Rev. Lett. 83 (1999) 1814.
[35] S. Khanna, F. Reuse, Chem. Phys. Lett. 205 (1993) 248.
[36] J. Niu, B.K. Rao, P. Jena, M. Manninen, Phys. Rev. B 51 (1995) 4475.
[37] F.D. Natterer, F. Patthey, H. Brune, Inspecting the Nuclear Spin State of Hydrogen Molecules with a Scanning Tunneling Microscope, 2013. (in preparation).
[38] P. Redhead, Vacuum 12 (1962) 203.
[39] D.A. King, Surf. Sci. 47 (1975) 384.
[40] P.J. Barrie, Phys. Chem. Chem. Phys. 10 (2008) 1688.
[41] R. Gaisch, Scanning Tunneling Microscopy in Ultra-high Vacuum at Low Temperature , Ph.D. thesis Université de Lausanne, 1994.